N73-20935
NASA CR-2231

NASA CONTRACTOR REPORT

NASA CR-2231

SWIRLING JET TURBULENT MIXING AND COMBUSTION COMPUTATIONS

by Arthur Rubel

Prepared by
ADVANCED TECHNOLOGY LABORATORIES, INC.
Jericho, N.Y. 11753
for

NATIONAL AERONAUTICS AND SPACE ADMINISTRATION • WASHINGTON, D. C. • MARCH 1973

1. Report No.	2. Government Accession No.	3. Recipient's Catalog No.
NASA CR-2231		

4. Title and Subtitle	5. Report Date
SWIRLING JET TURBULENT MIXING AND COMBUSTION COMPUTATIONS	March 1973
	6. Performing Organization Code
7. Author(s)	8. Performing Organization Report No.
Arthur Rubel	ATL TR 180
	10. Work Unit No.
9. Performing Organization Name and Address	
Advanced Technology Laboratories, Inc. 400 Jericho Turnpike Jericho, New York 11753	11. Contract or Grant No. NASW-2075
	13. Type of Report and Period Covered
12. Sponsoring Agency Name and Address	Contractor Report
National Aeronautics and Space Administration Washington, D. C. 20546	14. Sponsoring Agency Code

15. Supplementary Notes

Project Manager, Cecil J. Marek, Airbreathing Engines Division, NASA Lewis Research Center, Cleveland, Ohio

16. Abstract

Computations are presented describing the mixing and combustion of swirling jets in a coaxial stream. It is demonstrated that the boundary layer equations represent the flow reasonably well until reversed flow is imminent. For the range of parameters investigated indications are that the edge velocity has little effect on the behavior of the flow. Furthermore, confining the flow with a constant pressure wall, or impressing a favorable pressure gradient on the coaxial flow, acts to reduce the severity of the centerline adverse pressure gradient created by the swirl decay. A simple scalar eddy viscosity model, including a potential core formulation, is shown to describe the behavior of weak swirling flow in the far region but is only in fair agreement with observations in the near region. The effects of swirl on a burning hydrocarbon jet exhausting into a cold coaxial stream are shown to be intensified by the reduction of the jet density due to combustion. The enhanced mixing properties of high swirl flow produce rapid diffusion of the burning gases into the cold edge flow causing early cessation of the NO producing reactions. Computations show that doubling the initial jet swirl could reduce the NO production by 25%.

17. Key Words (Suggested by Author(s))	18. Distribution Statement
Swirling flow Combustion Emissions	Unclassified - unlimited

19. Security Classif. (of this report)	20. Security Classif. (of this page)	21. No. of Pages	22. Price*
Unclassified	Unclassified	39	$3.00

* For sale by the National Technical Information Service, Springfield, Virginia 22151

TABLE OF CONTENTS

LIST OF FIGURES

LIST OF FIGURES (Continued)

LIST OF SYMBOLS

$\bar{C}_p$ - mixture specific heat at constant pressure

C_{p_k} - specific heat at constant pressure for species k

D - jet diameter

D_T - turbulent diffusion coefficient

F_s - eddy viscosity pre-multiplier

h_k - specific enthalpy of species k

k_T - turbulent thermal conductivity

M_k - molecular weight of species k

n - number of chemical species

N_{Le} - Lewis number; $\rho D_T/\mu D_T$

N_{Pr} - Prandtl number; $\mu_T \bar{C}_p/k_T$

N_{Ro} - Rossby number, u/w

p - pressure

r - radial coordinate

$r_{\frac{1}{2}}$ - half radius; $r_{\frac{1}{2}}=r_{edge}/2$

R - jet radius

$\bar{R}$ - universal gas constant

R_i^* - Richardson number; $\dfrac{\frac{1}{\rho}\frac{\partial \rho}{\partial r}\frac{w^2}{r}}{(\frac{\partial u}{\partial r})^2}$

$\bar{S}$ - swirl ratio; defined by Equation (16)

S^* - modified swirl ratio; note discussion following Equation (16)

T - temperature

u,U - axial velocity

v - radial velocity

w - tangential (swirl) velocity

$\dot{w}_k$ - mass rate of production of chemical species k

x - axial coordinate

α_k - mass fraction of chemical species k

μ_T - turbulent (eddy) viscosity

ρ - density

ψ - stream function

Ω - angular velocity; w/r

Subscripts

ℓ - centerline

e - edge

j - jet

w - wall

Page Intentionally Left Blank

SUMMARY

Computations are presented describing the mixing and combustion of swirling jets in a coaxial stream. It is demonstrated that the boundary layer equations represent the flow reasonably well until reversed flow is imminent.

An isothermal jet with initial solid body rotation and uniform axial velocity yield near region profiles of axial velocity that exhibit a maximum shifted from the axis for swirls less than that required for the onset of reversed flow. For the range of parameters investigated indications are that the edge velocity has little effect on the behavior of the flow. Furthermore, confining the flow with a constant pressure wall, or impressing a favorable pressure gradient on the coaxial flow, acts to reduce the severity of the centerline adverse pressure gradient created by the swirl decay.

A simple scalar eddy viscosity model, including a potential core formulation, is shown to describe the behavior of weak swirling flow in the far region but is only in fair agreement with observations in the near region. A slight modification of the model, employing radial uniformity of the eddy viscosity, is found to be sometimes advisable.

The effects of swirl on a burning hydrocarbon jet exhausting into a cold coaxial stream are shown to be intensified by the reduction of the jet density due to combustion. The enhanced mixing properties of high swirl flow produce rapid diffusion of the burning gases into the cold edge flow causing early cessation of the NO producing reactions. Computations show that doubling the initial jet swirl could reduce the NO production by 25%.

INTRODUCTION

There are two important features that distinguish the turbulent mixing of swirling streams from the mixing of non-rotating flows. The streams mix in a distance that can be different from that associated with the corresponding non-rotating streams and may be thought of as resulting from an effective change in the system eddy viscosity. Furthermore, swirling jets with a sufficient flux of angular momentum may experience adverse axial pressure gradients severe enough to cause reversed (recirculating) flow. The scope of this study is limited to eddy viscosity effects and adverse pressure gradient effects only up to the point at which recirculation is first encountered.

Because the mixing processes are so important in combustion situations it is not surprising that many of the observations on the effects of swirl have been with respect to the improvement of burning characteristics. Schwartz (Reference 1) demonstrated that rotating a propane-air mixture in an annular combustion chamber and exhausting to ambient air results in appreciable shortening of the flame length, increased flame divergence, improved stability characteristics and delayed blow-off.

Chervinsky (Reference 2) analyzed a turbulent diffusion flame with swirl. He also found that the flame length was reduced and the flame stabilized when the fuel jet swirl was increased. Chervinsky deduced that the addition of swirl increased the eddy viscosity and altered the turbulent Prandtl number.

The set of experiments carried out by Fejer, Hermann and Torda (Reference 3) have provided a description of the mixing region velocity profiles for a swirling air jet exhausting into a non-rotating coaxial airstream under isothermal conditions. This data shows improved mixing due to rotation and is particularly helpful since zero swirl cases are presented which allow direct comparison between swirling and non-swirling flows. The data of Reference (3) also includes regimes of recirculating flow and indicates the existence of jet exit plane profile distortion even prior to the establishment of reversed flow. When recirculation appeared reversed flow was detected at the jet exit plane. Such regions are of obvious importance, in flame stabilization and have been studied in some detail by Syred, Chigier and Beér (Reference 4).

Beer and Chigier (Reference 5) have shown that when a turbulent diffusion flame is confined within a rotating environment then the flame length is increased, the flame speed is reduced and the boundary of the flame is laminarized. It was concluded that the interaction of density gradients with the rotating field was responsible for this behavior and for a modified Richardson number greater than unity the turbulence of the system can be damped. The definition of the modified Richardson number, R_i^* is given in terms of local parameters by

$$R_i^* = \frac{\frac{1}{\rho}\frac{\partial \rho}{\partial r}\frac{w^2}{r}}{\left(\frac{\partial u}{\partial r}\right)^2}$$

This formulation assumes an invariant rotational force field. Lilley (Reference 6) defines the Richardson number as a function of the radial angular momentum gradient such that a Prandtl type mixing length is increased where the gradient is negative and decreased when the gradient is positive. For constant density flows this behavior is consistent with the formulation of Rubel (Reference 7).

In that model increased mixing due to swirl is attributed to a mechanism of rotational instability governed by the local criterion

$$\frac{\partial}{\partial r}(\rho r^4 \Omega^2) \begin{cases} > & \text{stable} \\ = 0 & \text{neutral} \\ < & \text{unstable} \end{cases}$$

A correction factor for the eddy viscosity of such flows in the form of the pre-multiplier $(1 + 90/N_{Ro}^2)^{1/2}$ was used to quantitatively describe the relationship between mixing and swirl.

The purpose of this report is to present some computations describing swirling jet mixing and combustion. A jet with uniform axial velocity and solid body rotation exhausting into a non-rotating coaxial stream is examined as the jet rotation is increased until reversed flow is about to begin. The value of the swirl ratio, S^*, at separation as well as the general nature of the flow in the moderate swirl regime are in agreement with observations (References 3 and 8).

In addition, the simple eddy viscosity model of Reference (7), modified to account for a potential core, is shown to give fair agreement with the weak swirl data of Reference (3) in the near region and good agreement in the far region ($x/D > 15$). Finally, finite rate chemistry calculations are performed to demonstrate a manner in which swirling flow can be utilized to reduce pollutants generated by the combustion process. In the case presented, the swirl induced rapid mixing of combustion gases with the cooler coaxial air flow reduces the NO production by 25%. The geometry used for these calculations has the basic features of the swirl-can combustor currently under development at NASA Lewis (Reference 9).

GOVERNING EQUATIONS

The problem being described here is a turbulent swirling jet exhausting into a coaxial non-rotating stream. The stream can be confined or free and the possibility of combustion exists. The governing equations used are:

Conservation of Global Mass

$$\frac{\partial}{\partial x}(\rho u r) + \frac{\partial}{\partial r}(\rho v r) = 0 \tag{1}$$

Conservation of Species Mass

$$\rho u \frac{\partial \alpha_k}{\partial x} + \rho v \frac{\partial \alpha_k}{\partial r} = \frac{1}{r}\frac{\partial}{\partial r}\left(\mu_T \frac{N_{Le}}{N_{Pr}} r \frac{\partial \alpha_k}{\partial r}\right) + \dot{w}_k, \quad k=1, n \tag{2}$$

Conservation of Axial Momentum

$$\rho u \frac{\partial u}{\partial x} + \rho v \frac{\partial u}{\partial r} = -\frac{\partial p}{\partial x} + \frac{1}{r}\frac{\partial}{\partial r}\left(\mu_T r \frac{\partial u}{\partial r}\right) \tag{3}$$

Conservation of Radial Momentum

$$\rho r \Omega^2 = \frac{\partial p}{\partial r} \tag{4}$$

Conservation of Angular Momentum

$$\rho u \frac{\partial \Omega}{\partial x} + \rho v \frac{\partial \Omega}{\partial r} + 2\frac{\rho v \Omega}{r} = \frac{1}{r^3}\frac{\partial}{\partial r}\left(\mu_T r^3 \frac{\partial \Omega}{\partial r}\right) \tag{5}$$

Conservation of Energy

$$\begin{aligned} &\bar{C}_p \rho u \frac{\partial T}{\partial x} + \bar{C}_p \rho v \frac{\partial T}{\partial r} = u \frac{\partial p}{\partial x} + v \frac{\partial p}{\partial r} + \mu_T\left[\left(\frac{\partial u}{\partial r}\right)^2 + r^2\left(\frac{\partial \Omega}{\partial r}\right)^2\right] \\ &-\sum_k \dot{w}_k h_k + \frac{1}{r}\frac{\partial}{\partial r}\left[\frac{\bar{C}_p}{N_{Pr}}\mu_T r\left(\frac{\partial T}{\partial r} - \frac{r\Omega^2}{\bar{C}_p}\right)\right] \mu_T \frac{N_{Le}}{N_{Pr}}\frac{\partial T}{\partial r}\sum_k C_{p_k}\frac{\partial \alpha_k}{\partial r} \end{aligned} \tag{6}$$

The above equations result from making the boundary layer assumptions (e.g., Reference 10). The invoking of this simplification allows for the solution of the equations by numerical methods applicable to parabolic type partial differential equations. At the same time the use of such methods excludes the possibility of calculating recirculating flows.

These governing equations will be applied to situations that are very nearly recirculating. In these instances it is assumed that the radial penetration

of the conditions at the jet edge are primarily responsible for the behavior of the downstream flow field and that there is little influence from the downstream boundary conditions.

The turbulent transport properties of the flow are assumed to be functions of a scalar eddy viscosity, μ_T, and the turbulent Lewis and Prandtl numbers. The eddy viscosity pre-multiplier model of Rubel is used in conjunction with the potential core formulation of Kleinstein (Reference 11), so that

$$\mu_T = 0.00075\, F_s\, |\rho_e U_e - \rho_j U_j|\, x \qquad \text{(core)} \tag{7a}$$

$$\mu_T = 0.0286\, F_s\, r_{\frac{1}{2}}\, |\rho_e u_e - \rho_{\mathcal{L}}\, u_{\mathcal{L}}| \qquad \text{(downstream)} \tag{7b}$$

where

$$F_s(x,r) = 1 \text{ for } \frac{\partial}{\partial r}(\rho r^4 \Omega^2) > 0$$

$$F_s(x,r) = \left[1 + 90\left(\frac{1}{\rho}\right)_{\text{avg.}} \frac{(\rho_j r_j^2 \Omega_j^2)_{\max}}{(U_j - U_e)^2}\right]^{\frac{1}{2}} \text{ for } \frac{\partial}{\partial r}(\rho r^4 \Omega^2) \leq 0.$$

The core model is used until it matches the value of eddy viscosity given by the downstream model. The matching point occurs in a distance of from ten to twenty jet diameters and thereafter, the downstream model is used. In all the computations performed the Prandtl and Lewis numbers were taken to be unity.

The governing equations are cast into an (x,ψ) coordinate system by application of the von Mises transformation where

$$\rho u r = \psi \left(\frac{\partial \psi}{\partial r}\right)_x , \quad \rho v r = -\psi \left(\frac{\partial \psi}{\partial x}\right)_r \tag{8}$$

This transformation identically satisfies Equation (1) and recasts Equations (2) - (6) as

$$\frac{\partial \alpha_k}{\partial x} = \frac{1}{\psi}\frac{\partial}{\partial \psi}\left(\mu_T \frac{N_{Le}}{N_{Pr}} \frac{\rho u r^2}{\psi} \frac{\partial \alpha_k}{\partial \psi}\right) + \frac{\dot{w}_k}{\rho u} \quad , k=1, n \tag{9}$$

$$\frac{\partial u}{\partial x} = -\frac{1}{\rho u}\frac{\partial p}{\partial x} + \frac{1}{\psi}\frac{\partial}{\partial \psi}\left(\mu_T \frac{\rho u r^2}{\psi} \frac{\partial u}{\partial \psi}\right) + \frac{v r \Omega^2}{u^2} \tag{10}$$

$$\frac{\psi \Omega^2}{u} = \frac{\partial p}{\partial \psi} \tag{11}$$

$$\frac{\partial \Omega}{\partial x} = -\frac{2v\Omega}{ru} + \frac{1}{r^2 \psi}\frac{\partial}{\partial \psi}\left(\mu_T \frac{\rho u r^4}{\psi} \frac{\partial \Omega}{\partial \psi}\right) \tag{12}$$

$$\bar{C}_p \frac{\partial T}{\partial x} = \frac{1}{\rho} \frac{\partial p}{\partial x} + \frac{\rho u r^2}{\psi^2} \mu_T \left[\left(\frac{\partial u}{\partial \psi} \right)^2 + r^2 \left(\frac{\partial \Omega}{\partial \psi} \right)^2 + \frac{N_{Le}}{N_{Pr}} \frac{\partial T}{\partial \psi} \sum_k C_{p_k} \frac{\partial \alpha_k}{\partial \psi} \right]$$

$$- \frac{1}{\rho u} \sum_k \dot{w}_k h_k + \frac{1}{\psi} \frac{\partial}{\partial \psi} \left[\mu_T \frac{\bar{C}_p r}{N_{Pr}} \left(\frac{\rho u r}{\psi} \frac{\partial T}{\partial \psi} - \frac{r \Omega^2}{\bar{C}_p} \right) \right] \tag{13}$$

which, along with the perfect gas law

$$p = \rho \bar{R} T \sum_k \frac{\alpha_k}{M_k} \tag{14}$$

completes the set of governing equations.

When the boundary conditions of α_k, u, Ω, T symmetry at the axis are applied to Equations (9), (10), (12) and (13) the l'Hospital rule is invoked, then, at the jet centerline

$$\frac{\partial \alpha_k}{\partial x} = 2\mu_T \frac{N_{Le}}{N_{Pr}} \frac{\partial^2 \alpha_k}{\partial \psi^2} + \frac{\dot{w}_k}{\rho u}, \quad k=1, n \tag{9a}$$

$$\frac{\partial u}{\partial x} = - \frac{1}{\rho u} \frac{\partial p}{\partial x} + 2\mu_T \frac{\partial^2 u}{\partial \psi^2} \tag{10a}$$

$$\frac{\partial \Omega}{\partial x} = \frac{\Omega}{\rho u} \frac{\partial (\rho u)}{\partial x} + 4\mu_T \frac{\partial^2 \Omega}{\partial \psi^2} \tag{12a}$$

$$\bar{C}_p \frac{\partial T}{\partial x} = \frac{1}{\rho} \frac{\partial p}{\partial x} - \frac{1}{\rho u} \sum_k \dot{w}_k h_k + 2 \frac{\mu_T \bar{C}_p}{N_{Pr}} \frac{\partial^2 T}{\partial \psi^2} \tag{13a}$$

The initial and boundary conditions for the coaxial jet are

$$\begin{aligned}
&x=0: \ \alpha_k = \alpha_{k_j}(\psi), \ u = u_j(\psi), \ \Omega = \Omega_j(\psi), \ T = T_j(\psi), \\
&\qquad r_w \text{ or } p_w \\
&\psi=0: \ \frac{\partial \alpha_k}{\partial \psi} = \frac{\partial u}{\partial \psi} = \frac{\partial \Omega}{\partial \psi} = \frac{\partial T}{\partial \psi} = 0 \\
&\psi=\psi_e: \ \alpha_k = \alpha_{k_e}, \ u = u_e, \ \Omega = 0, \ T = T_e \qquad \begin{cases} p(\psi_w) = p_w(x) \\ \text{or} \\ r(\psi_w) = r_w(x) \end{cases} \\
\text{or} \quad &\psi=\psi_w: \ \frac{\partial \alpha_k}{\partial \psi} = \frac{\partial u}{\partial \psi} = \frac{\partial \Omega}{\partial \psi} = 0, \ \frac{\partial T}{\partial \psi} = \frac{\psi \Omega^2}{\rho u \bar{C}_p} \qquad \end{aligned} \tag{15}$$

Here, the initial jet profiles and edge conditions are to be specified including either the pressure distribution $p_w(x)$, on the streamline originally located at r_w or the location of the streamline, $r_w(x)$, with initial pressure p_w. Until the wall begins to interfere with the jet inviscid relationships govern the edge conditions. When the wall begins to interfere with the jet then zero net transport across the wall is assumed.

The governing system of partial differential equations was solved numerically by the explicit finite-difference technique of Zeiberg and Bleich (Reference 12) altered to consider the presence of angular momentum and radial pressure gradients. The forward marching procedure is begun at the wall or edge streamline where the axial pressure gradient is known (prescribed or assumed). In order to continue this scheme the axial pressure gradient along the neighboring streamline must be obtained. This is found by inward integration of the radial momentum equation. The technique can now be continued along each streamline to the axis. Where a value for the radial velocity is required it is computed from the streamline deflection, i.e., $v = u(\partial r/\partial x)_\psi$, using backward differences. At the start of the calculation the radial velocity is assumed to be zero.

In the case where the edge streamline position is prescribed the associated pressure must be iterated upon for each axial step. The iteration is completed when the assumed pressure results in a streamline position that is in agreement with the prescribed position to within one percent of the radial mesh width.

The basic concepts of Ferri, Moretti and Slutsky (Reference 13) have been applied to numerically couple the mixing and finite rate chemistry equations.

RESULTS AND DISCUSSION

A computer program developed at ATL based upon the analysis given above was used to determine the effect of several parameters on the behavior of a swirling jet exhausting into a coaxial stream and to explore application of these principles to combustor studies.

Isothermal Jet With Uniform Initial Conditions - This example was chosen so that the basic behavior of a swirling jet could be studied and the influence of various parameters ascertained. A 2.54 cm diameter jet with uniform axial velocity of 122 m/sec and solid body rotation is assumed to be exhausting into a 31 m/sec non-rotating coaxial stream bounded by a 15.24 cm diameter wall. The pressure and temperature of the streams are 1 atmosphere and 300K respectively. These conditions have integral properties similar to those of Reference (3).

The effect of swirl on the axial velocity decay at the centerline is shown in Figure (1). An adverse pressure gradient, created by the decaying swirl field, slows the flow increasingly as a function of initial swirl up to $R\Omega_j/U_j = 49/48$. Further increases in swirl caused failure of the program due to reversed flow. Increased swirl enhances mixing since the eddy viscosity is greater (unstable angular momentum distribution) and, for $U_e/U_j < 1$, the reduced centerline axial velocity is also in the direction of the final fully mixed solution.

In Figure (2) the streamlines are plotted for the $R\Omega_j/U_j = 49/48$ case (note stretched radial coordinate) and demonstrate the deflection of streamlines near the region of reduced axial velocity. One can anticipate the separation zone that will appear upon further increase of the deflection of the streamlines near the axis.

For the initial profiles and eddy viscosity model selected here the effects of adverse pressure gradient crest at $x/D \approx 5$. The radial distribution of axial velocity at this location is shown in Figure (3) as a function of $R\Omega_j/U_j$. The effects of increased rates of mixing extend the mixing zone to greater radial distances with increased swirl. At the same time the adverse axial pressure gradient causes the maximum velocity to be shifted away from the axis for $R\Omega_j/U_j > 3/4$.

The downstream development of the axial velocity distribution is given in Figure (4) for $R\Omega_j/U_j = 1$. The maximum velocity has been shifted from the centerline within one diameter of the jet exit plane. The bulge in the profile grows until $x/D \approx 5$ where the shear forces begin to dominate the inner region and eventually return the profile to that of ordinary mixing ($x/D \approx 10$).

The distribution of angular velocity with downstream distance for $R\Omega_j/U_j = 1$ (Figure 5) also has a peak away from the axis. Shear acts to reduce the angular velocity near the interface of the jet and edge stream but, in the nearly inviscid central region of the flow ($x/D > 5$) the angular velocity is also reduced. In this region the reduced axial velocity has caused the streamlines to be deflected outward (Figure 2). Since angular momentum (i.e.,

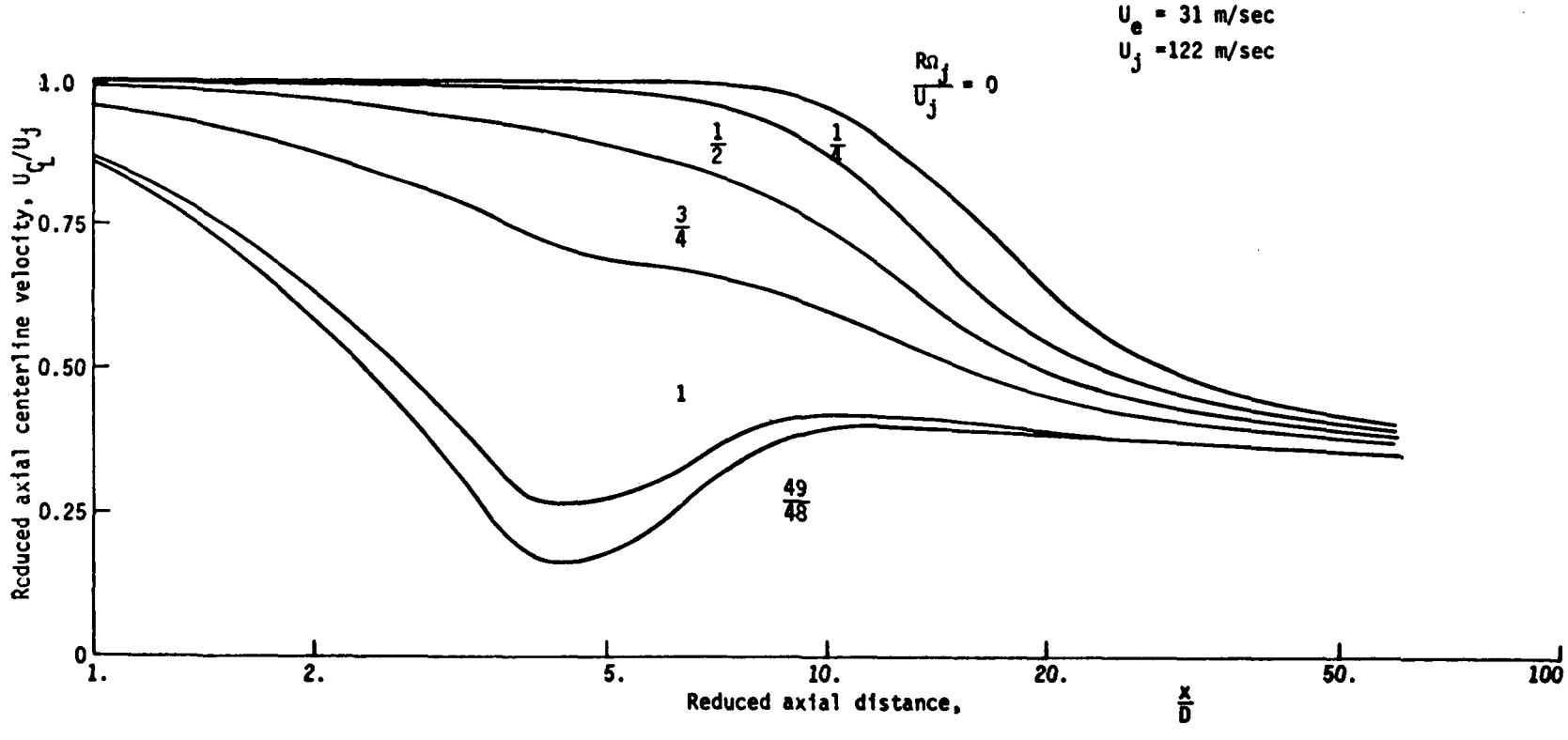

FIGURE 1. EFFECT OF SWIRL ON CENTERLINE AXIAL VELOCITY DECAY

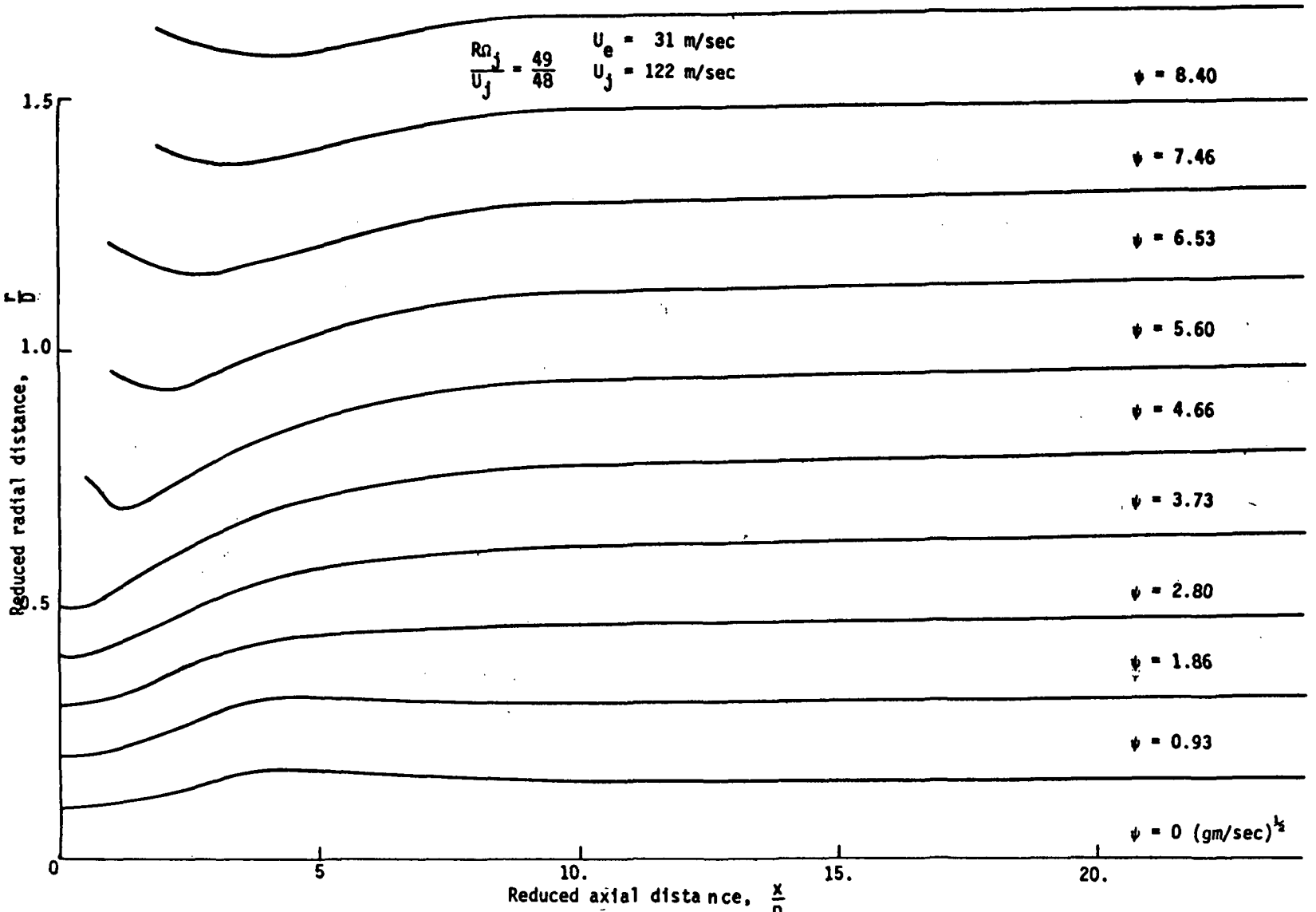

FIGURE 2. SWIRLING JET MIXING REGION STREAMLINES

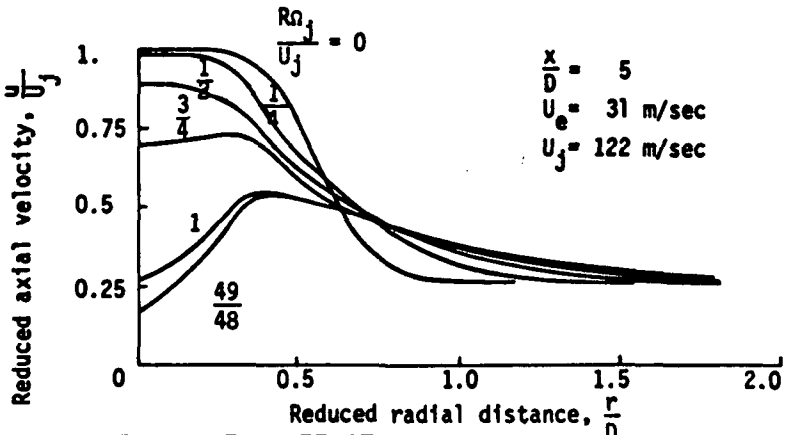

FIGURE 3. EFFECT OF SWIRL ON THE RADIAL DISTRIBUTION OF AXIAL VELOCITY

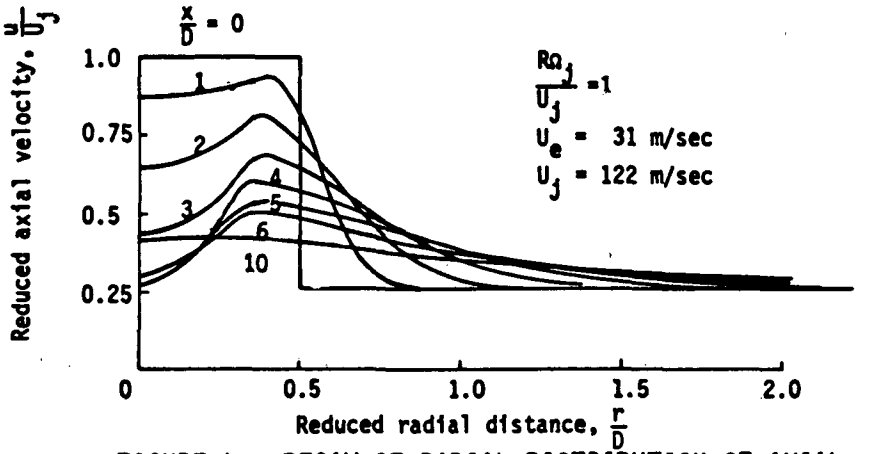

FIGURE 4. DECAY OF RADIAL DISTRIBUTION OF AXIAL VELOCITY

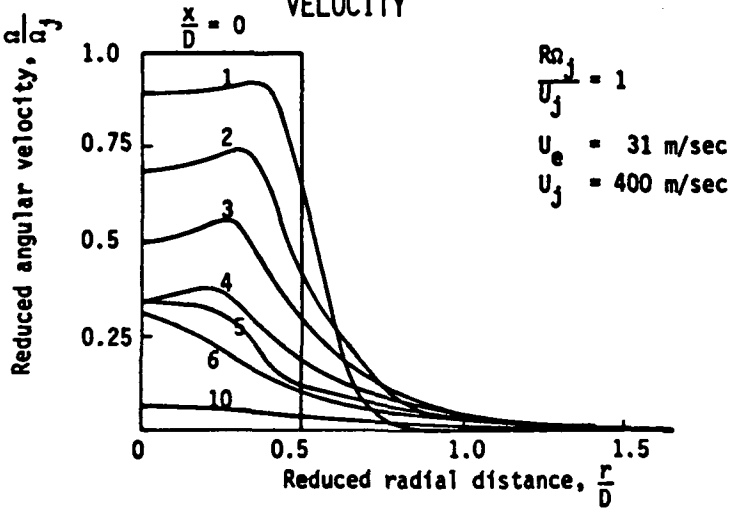

FIGURE 5. DECAY OF RADIAL DISTRIBUTION OF ANGULAR VELOCITY

$r^2\Omega$) along a streamline remains constant under these circumstances, then the angular velocity, Ω, along streamlines near the axis must be decreasing. The effects of shear begin to dominate the swirl behavior near the jet axis at $x/D \approx 5$ as was the case with the axial velocity.

The difference in pressure between the jet edge and centerline is another indication of the concentration of angular momentum within the jet. Figure (6) gives the axial decay of this pressure difference as a function of initial swirl. It appears that within five diameters of the jet exit plane there is little remaining of the initial radial pressure gradient. Since the length for decay is not much dependent upon the initial swirl, it follows that for nearly recirculating flows, the adverse pressure gradient impressed upon the flow at the axis is directly proportional to the initial pressure difference between the jet edge and centerline.

From these calculations the near flow field of a swirling jet exhausting into a coaxial stream can be described. Initially there is mixing at the interface of the jet and edge streams that acts to diffuse angular momentum from the jet. This diffusion acts to increase the pressure and, thus, to reduce the axial velocity throughout the jet. The streamlines move away from the centerline with the greatest deflections near the axis. This acts to further reduce the angular velocity near the jet centerline causing the most severe adverse pressure gradients to be located along the axis. It is for this reason that the axial velocity profile has its maximum shifted away from the axis. If the flow is not recirculating then shear gradients will begin to act at the centerline to increase the velocity before a stagnation point is attained, eventually producing the usual downstream mixing profile.

The effect of an exterior favorable pressure gradient on the behavior of the jet is shown in Figure (7). As expected, such a free stream gradient acts to reduce the centerline adverse pressure gradient. In the case presented here (i.e., p_w = 1-0.01575 x/D atmosphere) little velocity decrease is noted at the axis for initial swirl $R\Omega_j/U_j = 1$ and no reversed flow was encountered even for swirl as great as $R\Omega_j/U_j = 5/4$. The peak effects of swirl still appear to be restricted to within the first five jet diameters.

The effects of confining the jet are shown in Figure (8). Here the pressure at the confining wall was maintained constant and the initial wall radius was only twice the jet radius. The velocity profiles are unchanged (see Figures 4 and 5) until the wall interferes with the flow at $x/D > 2$. The wall reduces the diffusion of angular velocity which acts to delay the decay of the radial pressure gradient. The axial pressure gradient is made less severe so that the minimum velocity at the axis is greater than for the unconfined flow. Of course, the downstream results exhibit higher velocity since the amount of coaxial flow available for mixing is limited by the confinement.

The effects of the edge velocity on the swirling jet are indicated by Figure (9). Increasing the edge velocity from $U_e/U_j = 1/4$ to $U_e/U_j = 3/2$ had little effect on the value of the minimum velocity at the jet axis, but it did act to move this point toward the jet exit plane. The adverse axial pressure

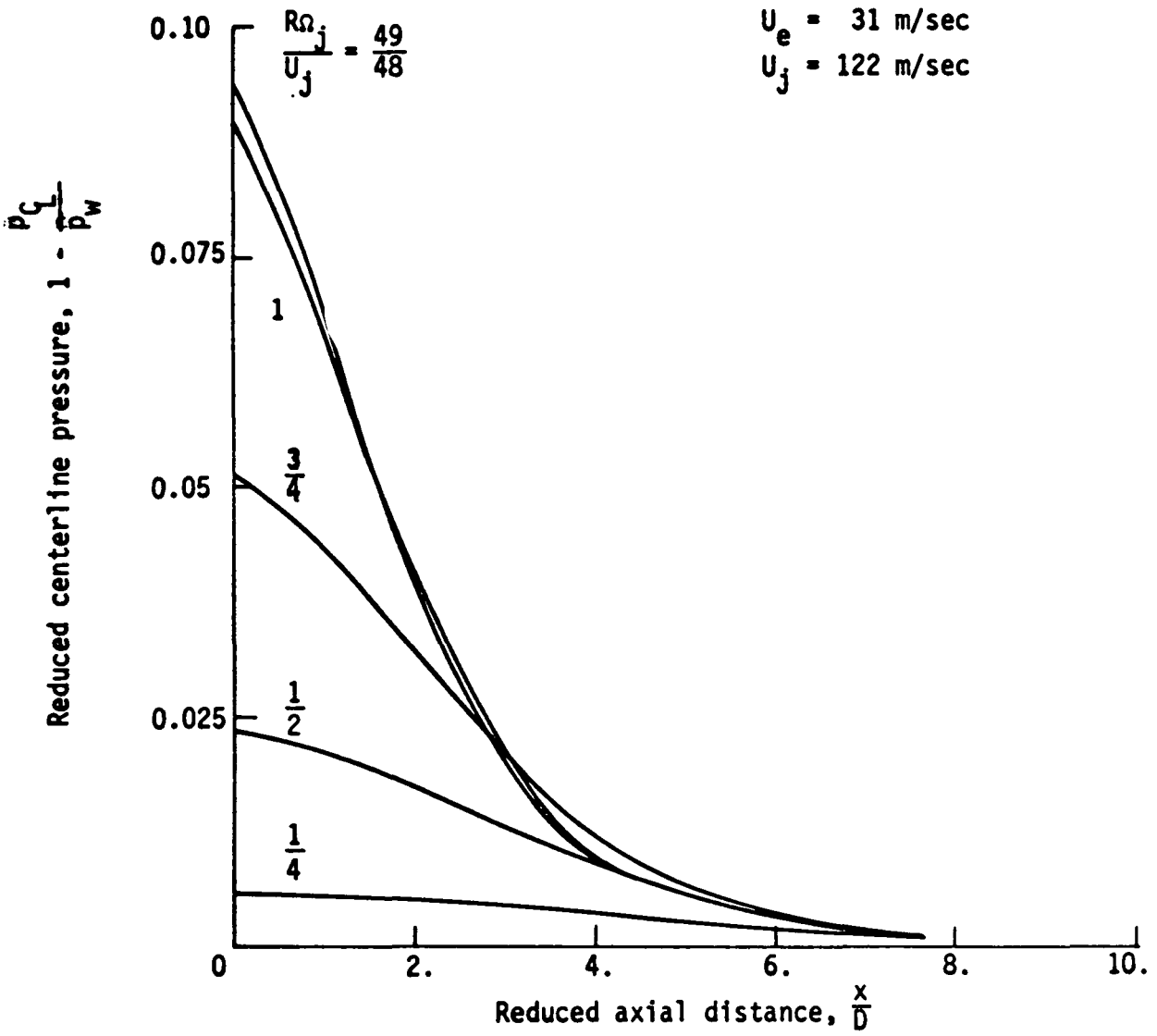

FIGURE 6. EFFECT OF SWIRL ON THE DECAY OF RADIAL PRESSURE DIFFERENCE

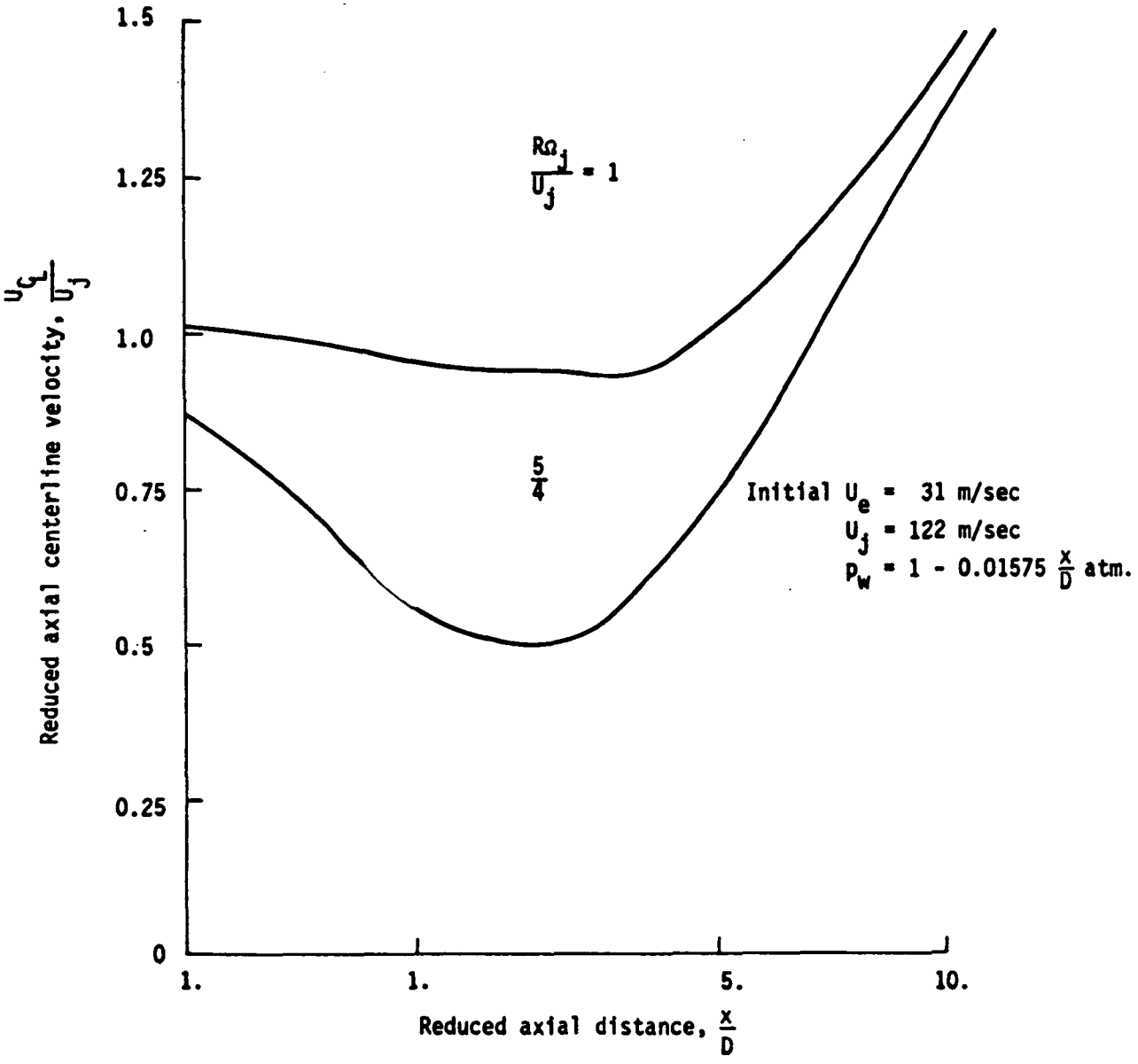

FIGURE 7. EFFECT OF SWIRL ON CENTERLINE AXIAL VELOCITY DECAY IN PRESENCE OF FAVORABLE EDGE PRESSURE GRADIENT

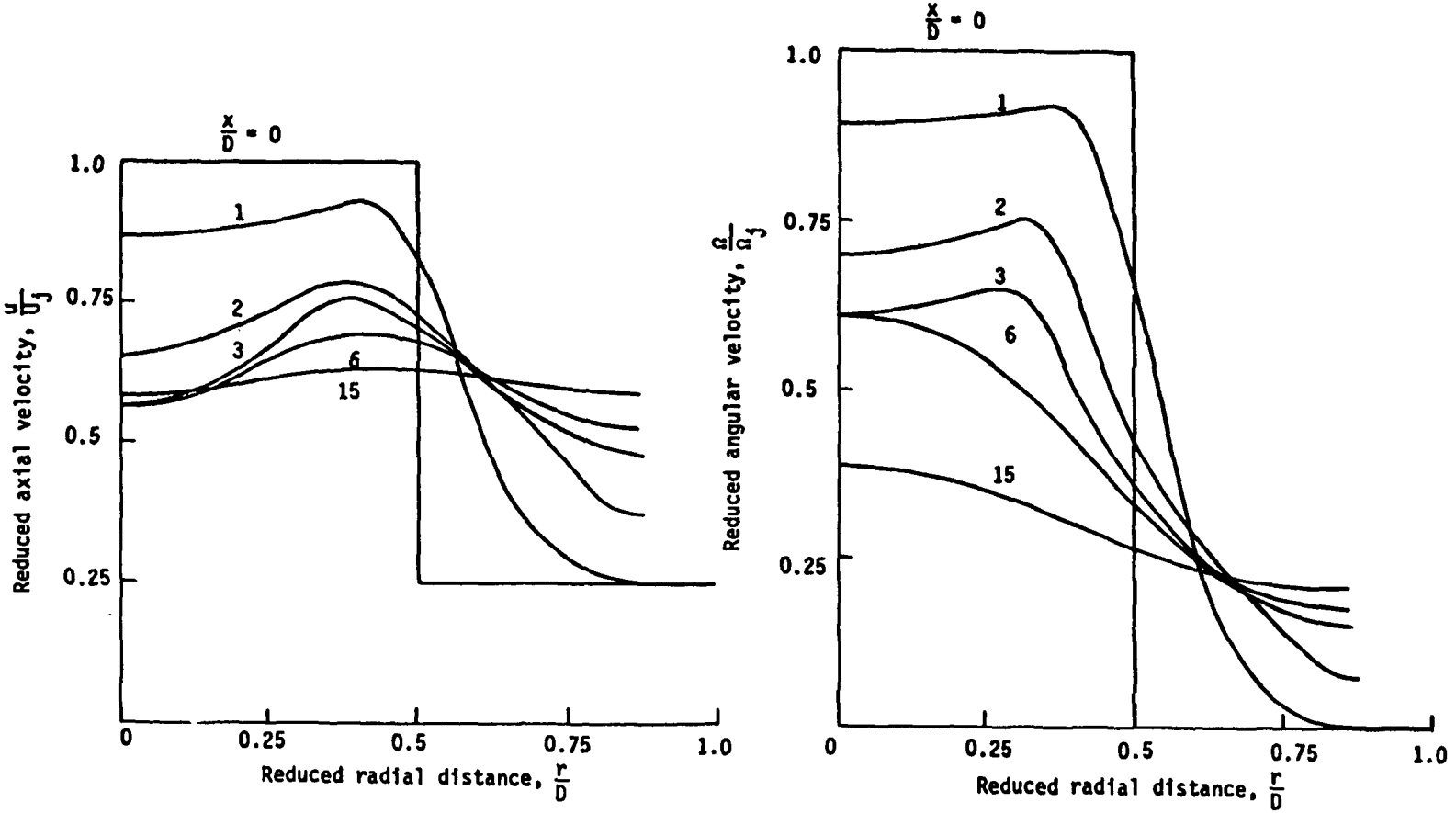

FIGURE 8. VELOCITY PROFILE DECAY WITH WALL INTERFERENCE
INITIAL $R_{WALL} = 2R$
$P_W = 1$ ATM

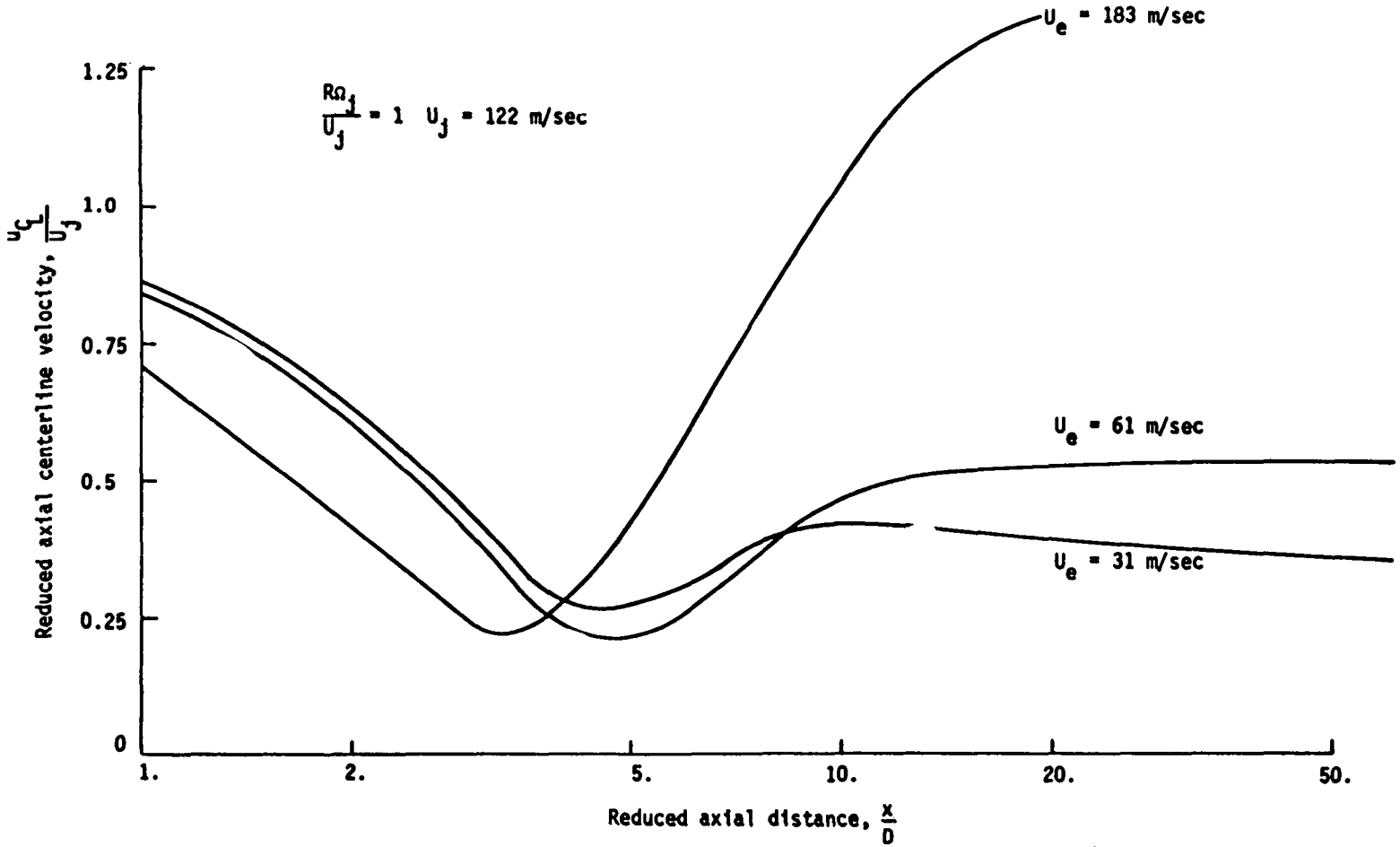

FIGURE 9. EFFECT OF EDGE VELOCITY ON CENTERLINE AXIAL VELOCITY DECAY

gradient at the axis is increased with increased edge velocity but axis shear gradients balance this effect.

Uniform initial profiles were used here as the simplest means of generating results for the effects of basic parameters on swirling jet behavior. These profiles preclude comparison with current data except, perhaps, on some integral basis. The characteristic parameter for describing swirling jets exhausting into a quiescent medium is the swirl parameter,

$$\bar{S} = \frac{\int_0^\infty \rho u r^3 \Omega dr}{R\left[\int_0^\infty u^2 r dr - \int_0^\infty (p_\infty - p)\, r dr\right]} \tag{16}$$

which is an invariant dimensionless ratio of angular momentum to axial momentum. Since $\bar{S}$ is no longer invariant when a coaxial stream is involved, it is necessary to define the parameter, S*, in the same manner as Equation (16) but with the jet radius, R as the outer limit of the integrals. This parameter reduces to $\bar{S}$ for the quiescent case but does not account for the presence of a coaxial stream. Since the edge velocity does not seem to influence the behavior of the near flow, except for slight displacement in the axial direction, this parameter may prove useful for prediction purposes (e.g., onset of flow reversal).

For uniform jet profiles of axial and angular velocity and constant density it is easy to demonstrate that

$$S^* = \left(\frac{2U_j}{R\Omega_j} - \frac{R\Omega_j}{2U_j}\right)^{-1} \tag{17}$$

The numerical computations have indicated that the maximum axial velocity begins to be displaced from the axis at $S^* \approx 0.43$ (Figure 3) and reversed flow is imminent at $S^* \approx 0.69$ (Figure 1). Chigier and Chervinsky (Reference 8) found these points to occur at $\bar{S} \approx 0.5$ and $\bar{S} \approx 0.6$, respectively for a tangential injection swirl generator. Of course, the jet exit plane profiles are also important in determining the downstream behavior of the flow. If the jet exit plane flow exhibits reduced velocity near the axis then one would expect flow reversal to occur at lower values of S* (calculated at the jet exit plane).

Decay Of A Swirling Jet With Nonuniform Initial Conditions - Computations of swirling jet flow were compared with some observations of Fejer et.al., (Reference 3) using the measured velocity profiles as the initial conditions for the calculations. The centerline decays of axial velocity for S* = 0, 0.14 (Cases 1a, 1b of Reference 3) are presented in Figure (10) and it is seen that the behavior of the non-rotating case is adequately described by the eddy viscosity formulation of Equations (7a) and (7b). For S* = 0 the velocity profiles are also well described by this model (Figure 11).

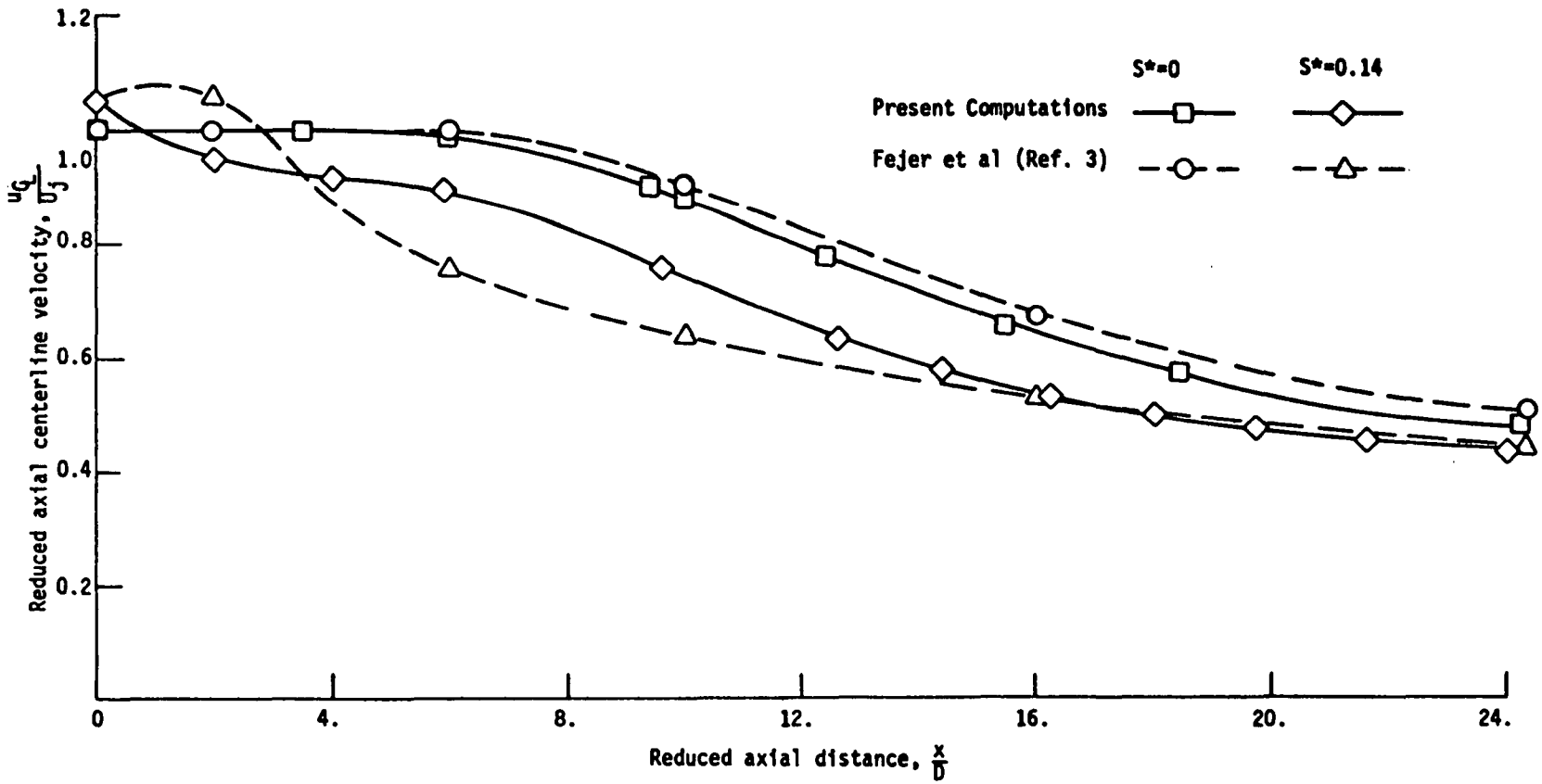

FIGURE 10. CENTERLINE DECAY OF AXIAL VELOCITY (NONUNIFORM INITIAL PROFILES)

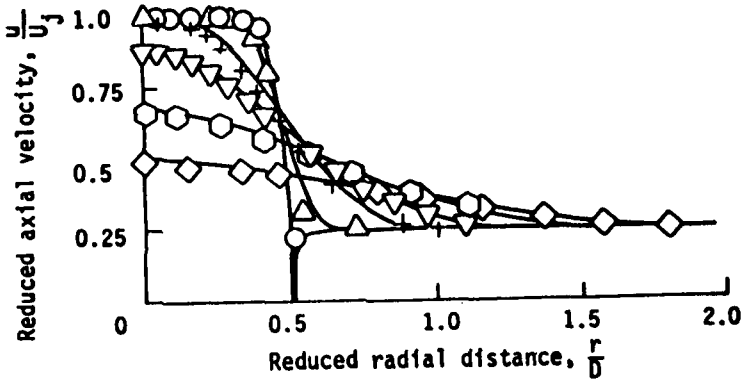

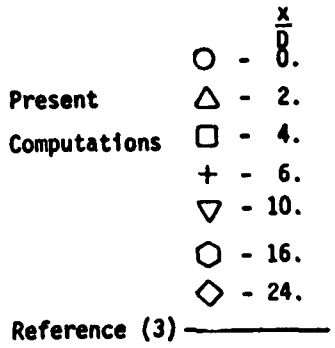

FIGURE 11. VELOCITY PROFILE DECAY, S*=0

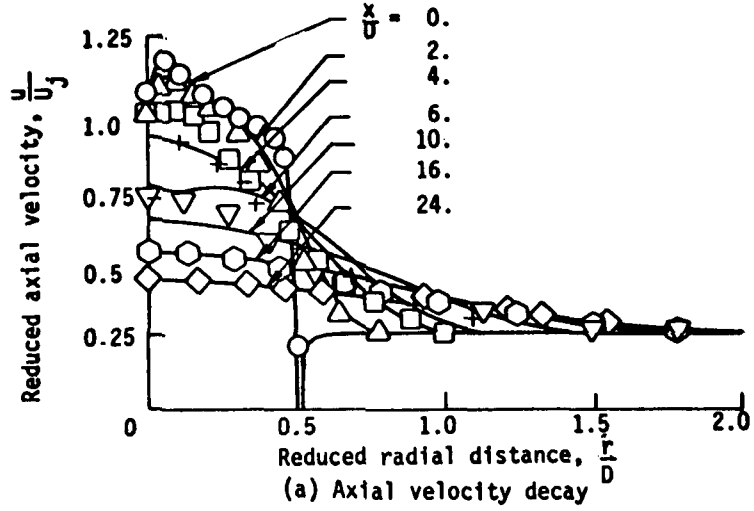

(a) Axial velocity decay

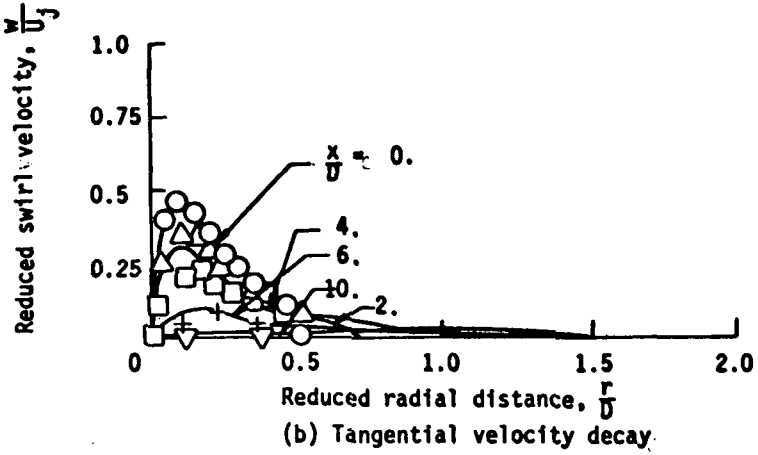

(b) Tangential velocity decay

FIGURE 12. VELOCITY PROFILE DECAY FOR $\mu=\mu(x,R)$, S*=0.14

For the case of weak swirl (S* = 0.14) only a fair description of the axial velocity decay in the first ten diameters is given by the pre-multiplier eddy viscosity model but downstream of x/D = 15 the agreement is excellent. The velocity profiles (Figure 12) are also in agreement beyond x/D = 15 and compare reasonably well in the outer mixing region, even for x/D < 15, but in the inner region the discrepancy is apparent.

The eddy viscosity model based on local rotational stability was modified so that, at any axial position x,

$$F_s(x) = 1 \quad \text{if} \quad \frac{\partial}{\partial r}(\rho r^4 \Omega^2) > 0 \quad \text{for all } r$$

$$F_s(x) = \left[1 + 90 \left(\frac{1}{\rho}\right)_{\text{avg.}} \frac{(\rho_j r_j^2 \Omega_j^2)_{max}}{(U_j - U_e)^2}\right]^{\frac{1}{2}} \quad \text{if} \quad \frac{\partial}{\partial r}(\rho r^4 \Omega^2) \leq 0 \text{ for any } r. \tag{18}$$

This model implies that at a given downstream location, if any segment of the flow is rotationally unstable then the eddy viscosity is increased over the entire jet width. Calculations using this model showed somewhat improved axial velocity profiles but increased the discrepancies between the swirl velocity profiles (Figure 13). Nevertheless, the more rapid decay of swirl given by the numerical computations is consistent with results presented in References (2) and (6). In order to fully describe both axial and swirl velocities a tensor eddy viscosity is inferred (e.g., Reference 6).

The radial behavior of eddy viscosity is especially important in nearly recirculating regions since shear gradients are, in general, responsible for increasing the axial velocity near the axis. Numerical calculations with initial conditions provided by the post-recirculation profiles of Reference (3)'s Case 1d, have indicated some superiority of the model $\mu=\mu(x)$ in this regime. Such a formulation also acts to delay the onset of reversed flow and can be used to bypass such regimes for some high swirl computations where downstream and outer region mixing are of primary importance. For this reason the pre-multiplier of Equation (18) is used for all further results presented here.

Applications To Finite Rate Combustion - In order to demonstrate some effects of jet swirl on the finite rate chemistry process, computations were made for a stoichiometric hydrocarbon-air jet exhausting into a channel of cold air. For comparison, two sets of calculations were performed differing only in swirl parameter (i.e., Case 1, S* = 0.36; Case 2, S* = 0.165). The geometry of the problem, as well as the initial conditions, are specified in Figures (14) and (15) and have basic parameters representative of the swirl-can design of Reference (9). The jet mixture is made ignitable by assuming that its exit plane temperature is 1130K. The chemical reactions used for the computations are given in Table I and their reaction rates can be found in References (14), (15) and (16).

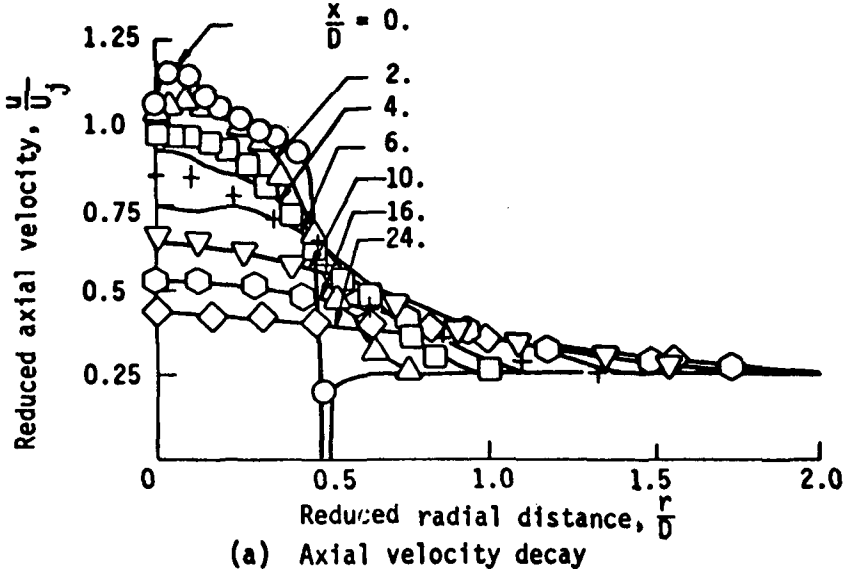

(a) Axial velocity decay

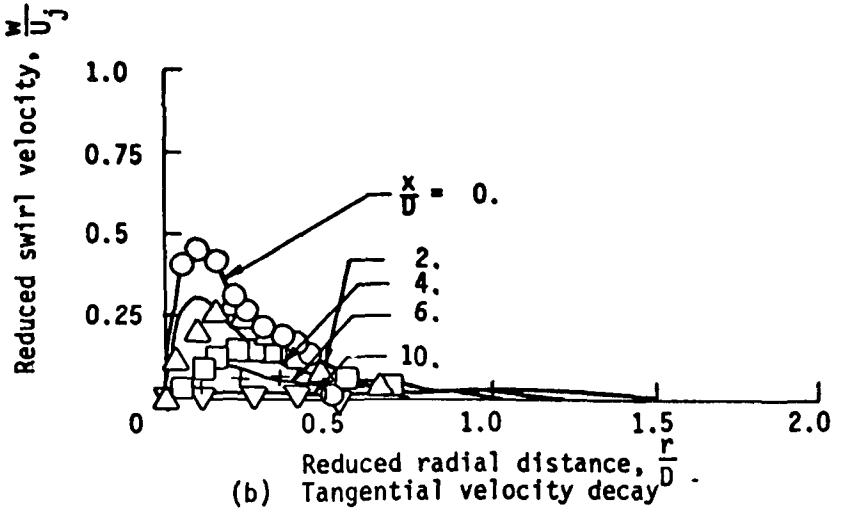

(b) Tangential velocity decay

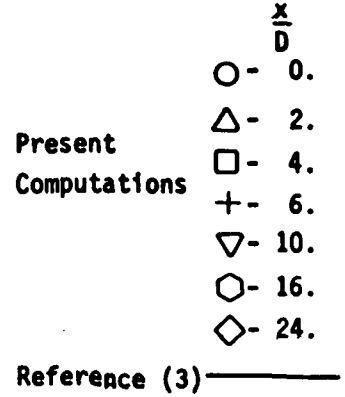

FIGURE 13. VELOCITY PROFILE DECAY FOR $\mu=\mu(x)$, $S^*=0.14$

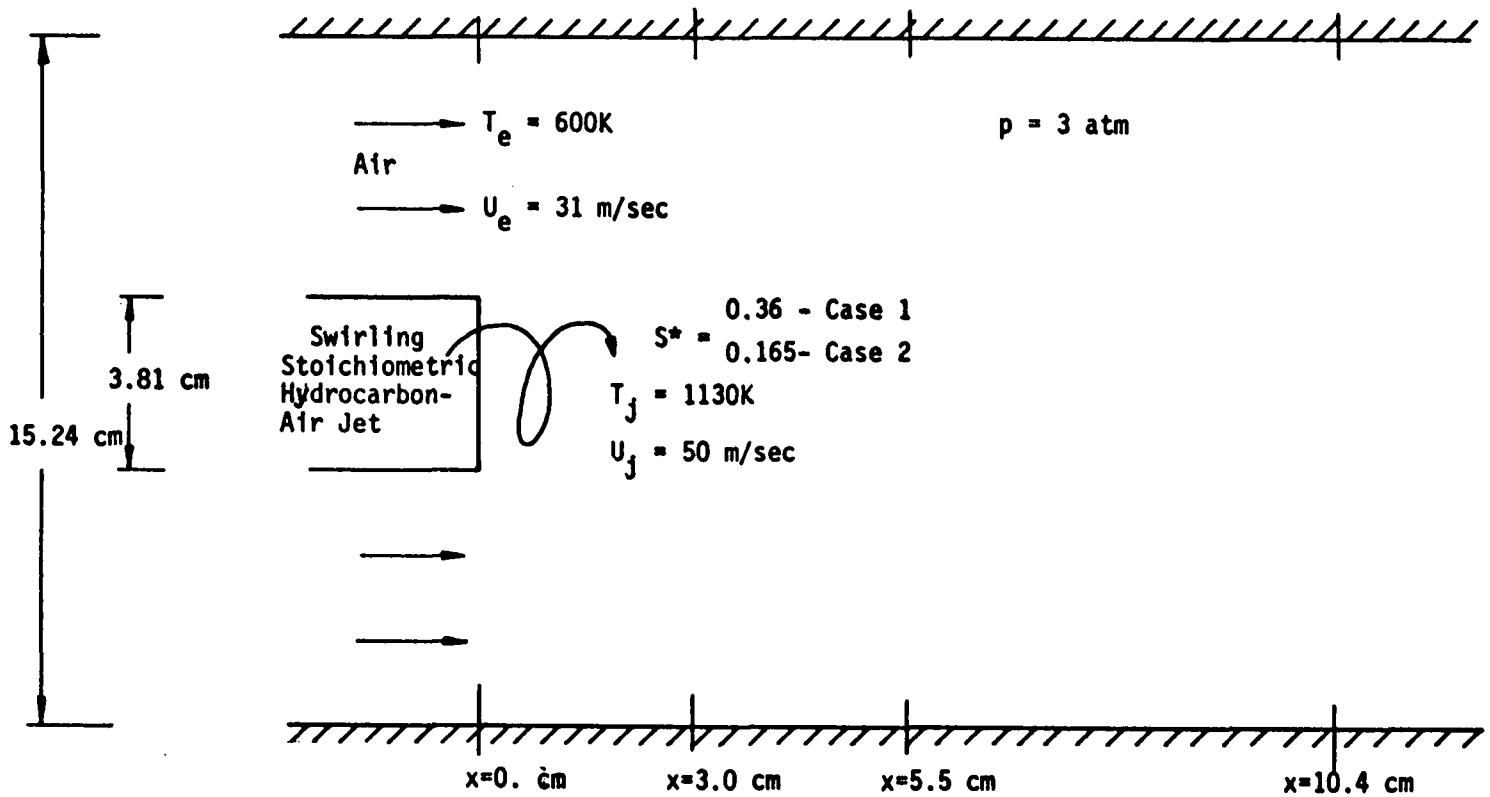

FIGURE 14. SCHEMATIC OF COAXIAL SWIRLING JET MIXING AND COMBUSTION

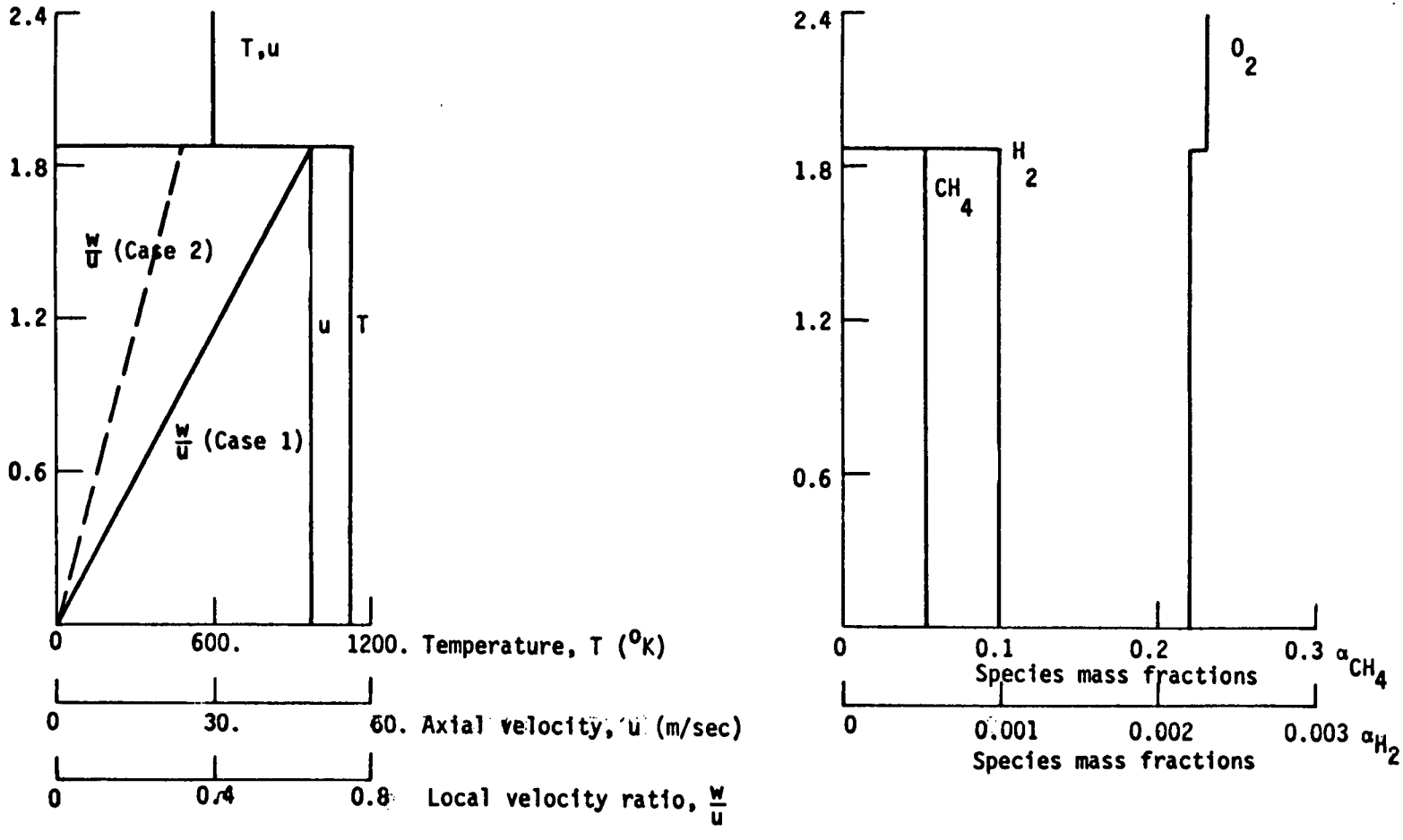

FIGURE 15. INITIAL PROFILES FOR CASE 1 AND CASE 2

TABLE I

CHEMICAL REACTION SYSTEM

$CH_4 + OH = CH_3 + H_2O$	$2OH = H_2O + O$
$CH_4 + O = CH_3 + OH$	$2O + X = O_2 + X$
$C_2H_4 + OH = CH_3 + CH_2O$	$H_2 + X = 2H + X$
$C_2H_4 + O = HCO + CH_3$	$CO + O_2 = CO_2 + O$
$CH_3 + O_2 = CH_2O + OH$	$CO + O + X = CO_2 + X$
$CH_2O + O = HCO + OH$	$N + N + X = N_2 + X$
$CH_2O + OH = HCO + H_2O$	$N + O + X = NO + X$
$HCO + O = OH + CO$	$N + NO = N_2 + O$
$HCO + OH = CO + H_2O$	$N + O_2 = NO + O$
$CO + OH = CO_2 + H$	$N + OH = NO + H$
$O_2 + H = OH + O$	$H + N_2O = N_2 + OH$
$O + H_2 = OH + H$	$O + N_2O = N_2 + O_2$
$H_2 + OH = H + H_2O$	$O + N_2O = NO + NO$

The temperature and velocity profiles at three axial stations for Case 1 are presented in Figures (16a), (16b) and (16c). At the low velocities used for these calculations combustion of the jet mixture is very rapid and at x = 3 cm the axis temperature has risen to 2700K. The swirl and axial velocities have profiles that are similar to those previously presented and show typical axial decays toward uniformity. The axial velocity profile exhibits a maximum away from the centerline even though $S^* < 0.43$. This is a result of the reduced density in the burning region. The adverse pressure gradient established by the swirl decay, when acting on fluid with reduced inertia, tends to produce the same flow patterns as in the isothermal cases, but at reduced values of S^*.

The mass fractions of the more important species are presented in Figures (17a), (17b) and (17c). It is to be noted that NO is being produced through much of the jet region, where the temperature is high. The local maximum of methane mass fraction appearing near the edge of the mixing region at 3 cm is due to methane that has diffused to a region of lower temperature wnere its combustion has been delayed.

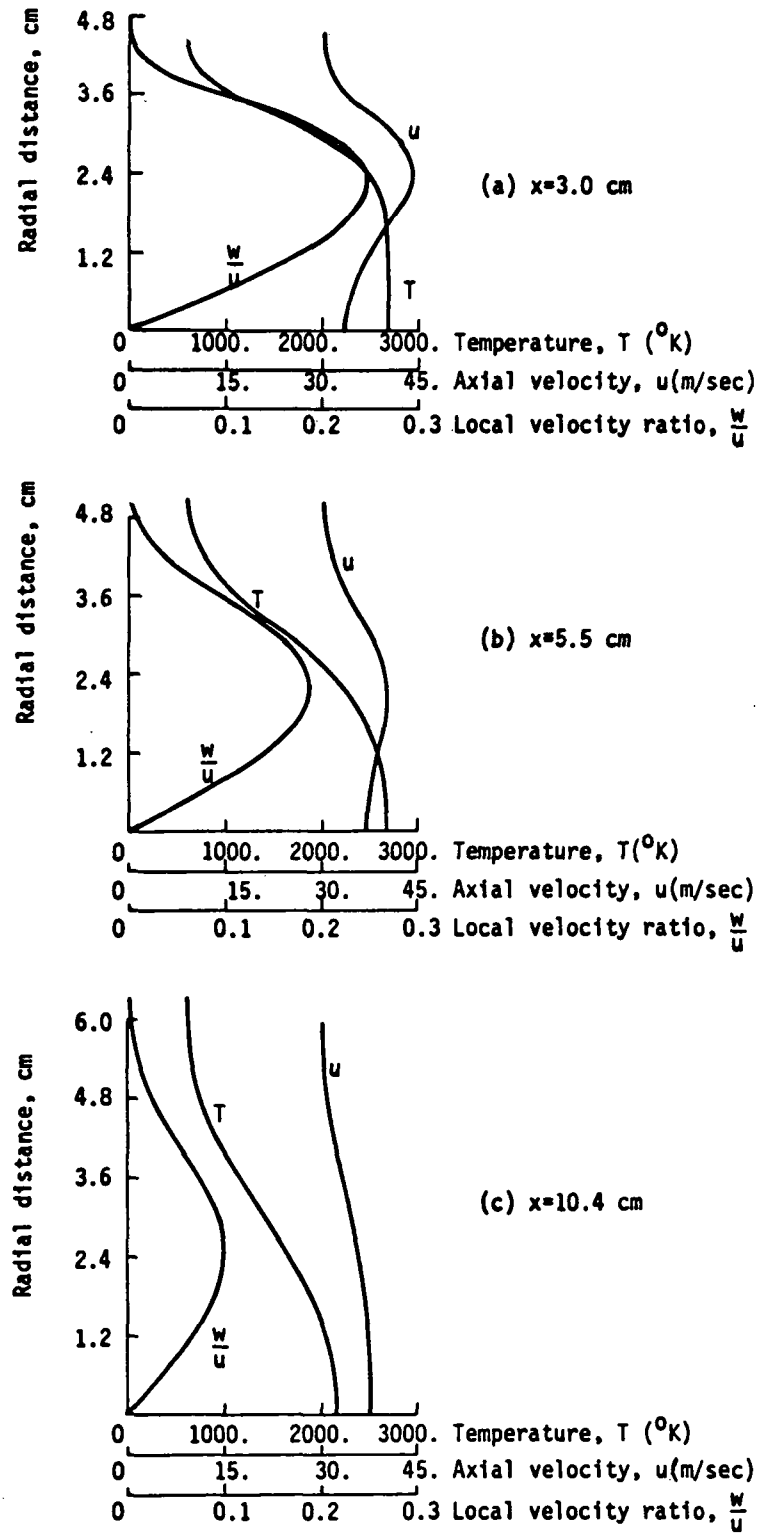

FIGURE 16. CASE 1 VELOCITY AND TEMPERATURE PROFILES ($S^*=0.36$)

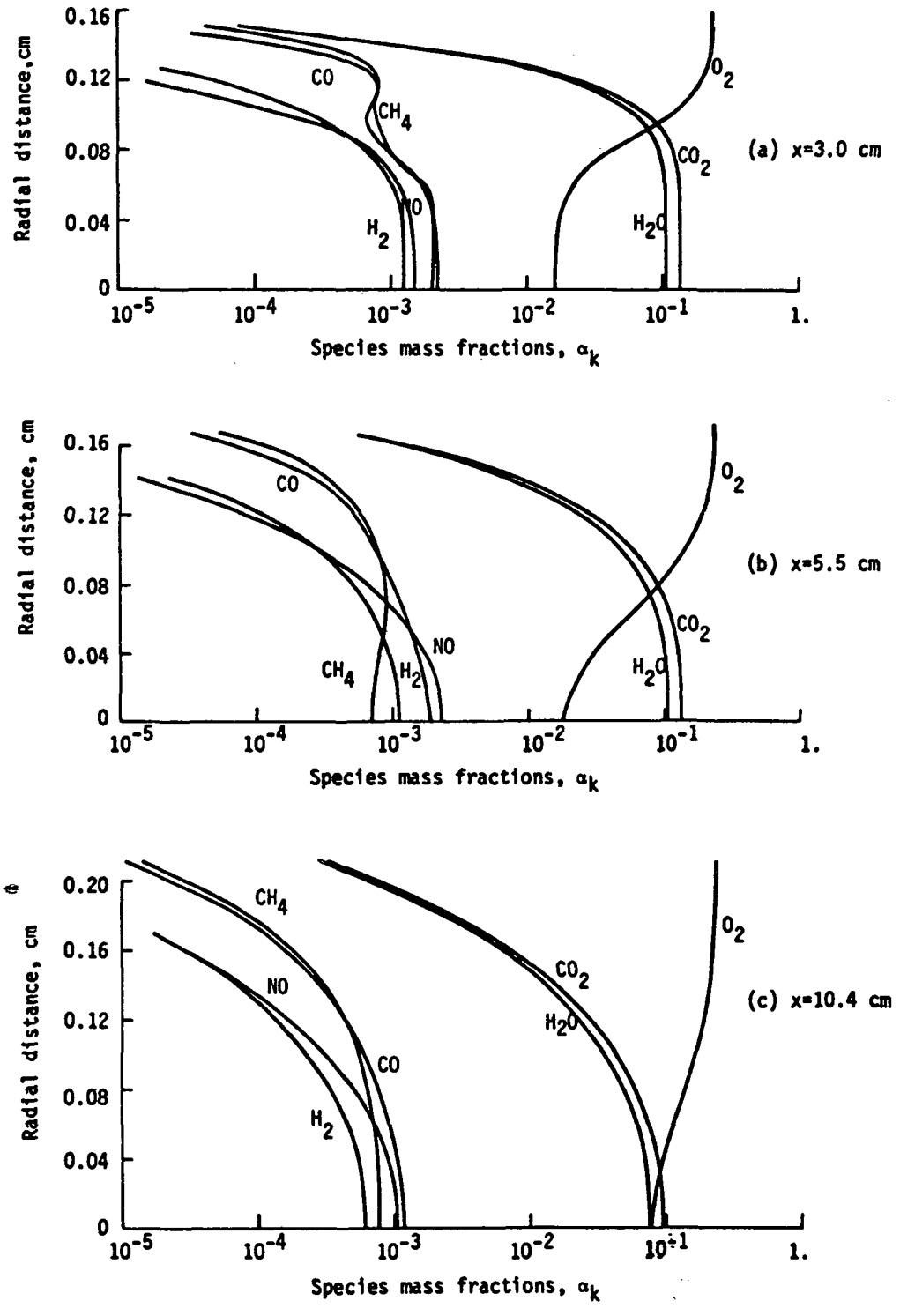

FIGURE 17. CASE 1 CHEMICAL SPECIES PROFILES (S^{*}=0.36)

The temperature and velocity profiles for Case 2, are presented in Figures (18a), (18b) and (18c). The swirl profiles are similar to those of Case 1 but reduced in scale. An axial velocity maximum of small proportion occurs away from the axis although the value of the swirl ratio is only $S^* = 0.165$.

The species distributions for Case 2 (Figures 19a, 19b and 19c) show behavior little different from those of Case 1 and are included for completeness.

The effect of swirl on overall pollutant production is shown in Figure (20). Here the emissions of CO and NO are shown for Cases 1 and 2 as a function of axial distance. The CO production curves are almost identical for the two cases. Burning takes place earlier for the high swirl case because of the reduced jet velocity and, therefore, the CO production curve for $S^* = 0.165$ slightly lags that for $S^* = 0.36$. The behavior of the NO production curves is somewhat different. Until $x \approx 4$ cm there is more NO produced by the high swirl case due to the longer residence times. The reactions producing NO, however, are relatively slow and highly temperature dependent. Thus, the increased mixing due to increased swirl more rapidly diffuses the burned gases into the cold edge stream causing an earlier cessation of NO production. For the two cases calculated here the NO production was reduced by 25% upon doubling the initial swirl.

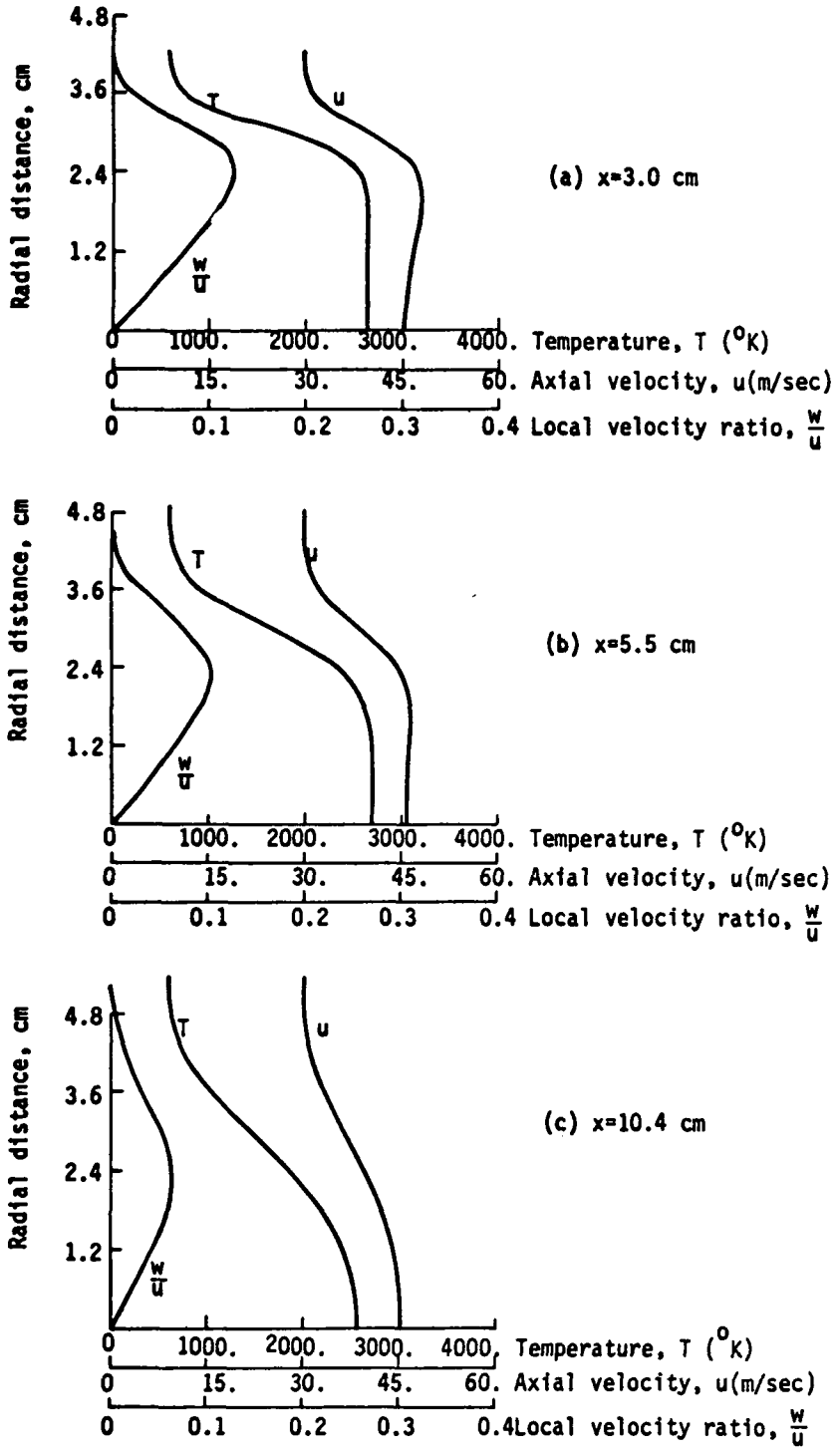

FIGURE 18. CASE 2 VELOCITY AND TEMPERATURE PROFILES (S^*=0.165)

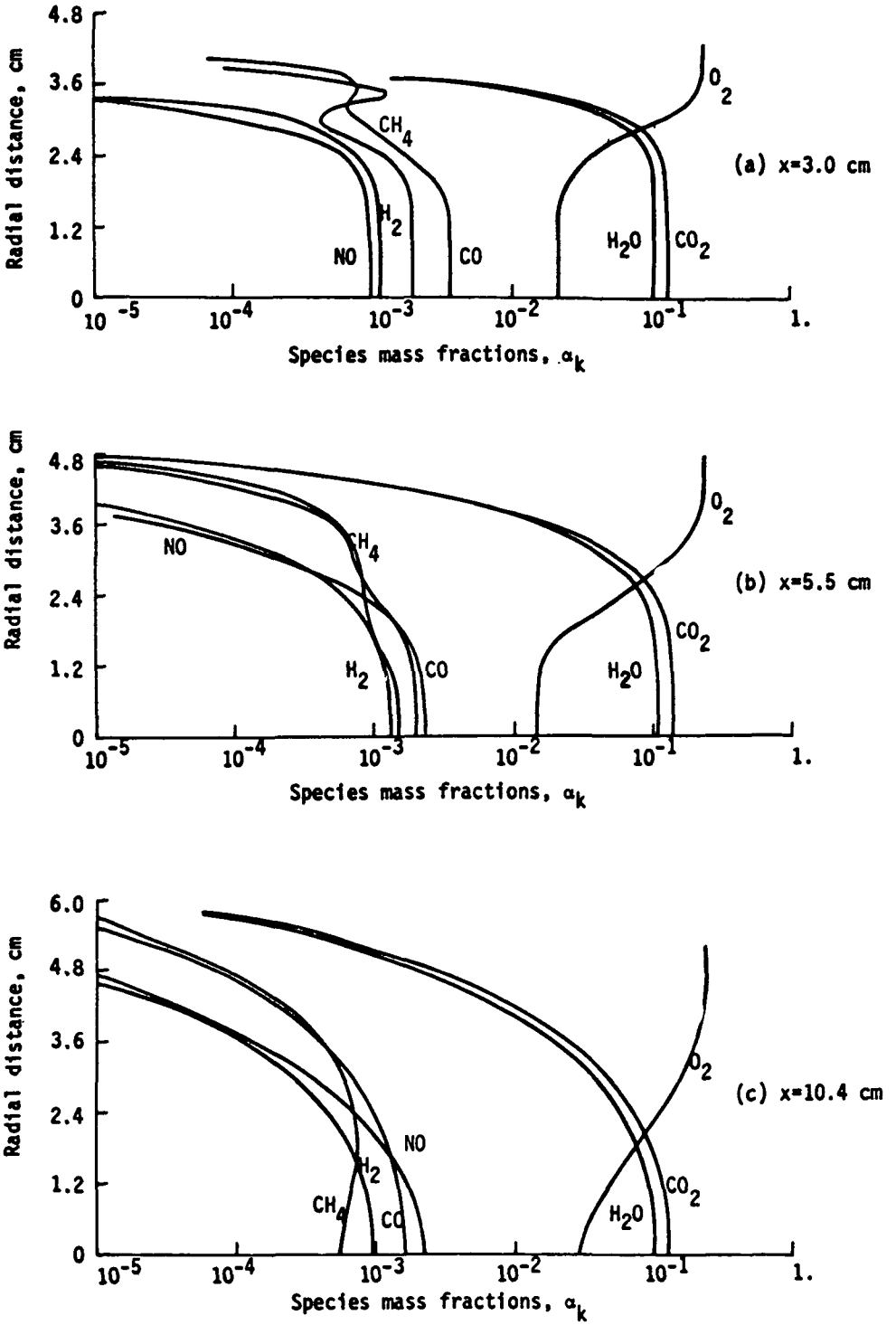

FIGURE 19. CASE 2 CHEMICAL SPECIES PROFILES (S*=0.165)

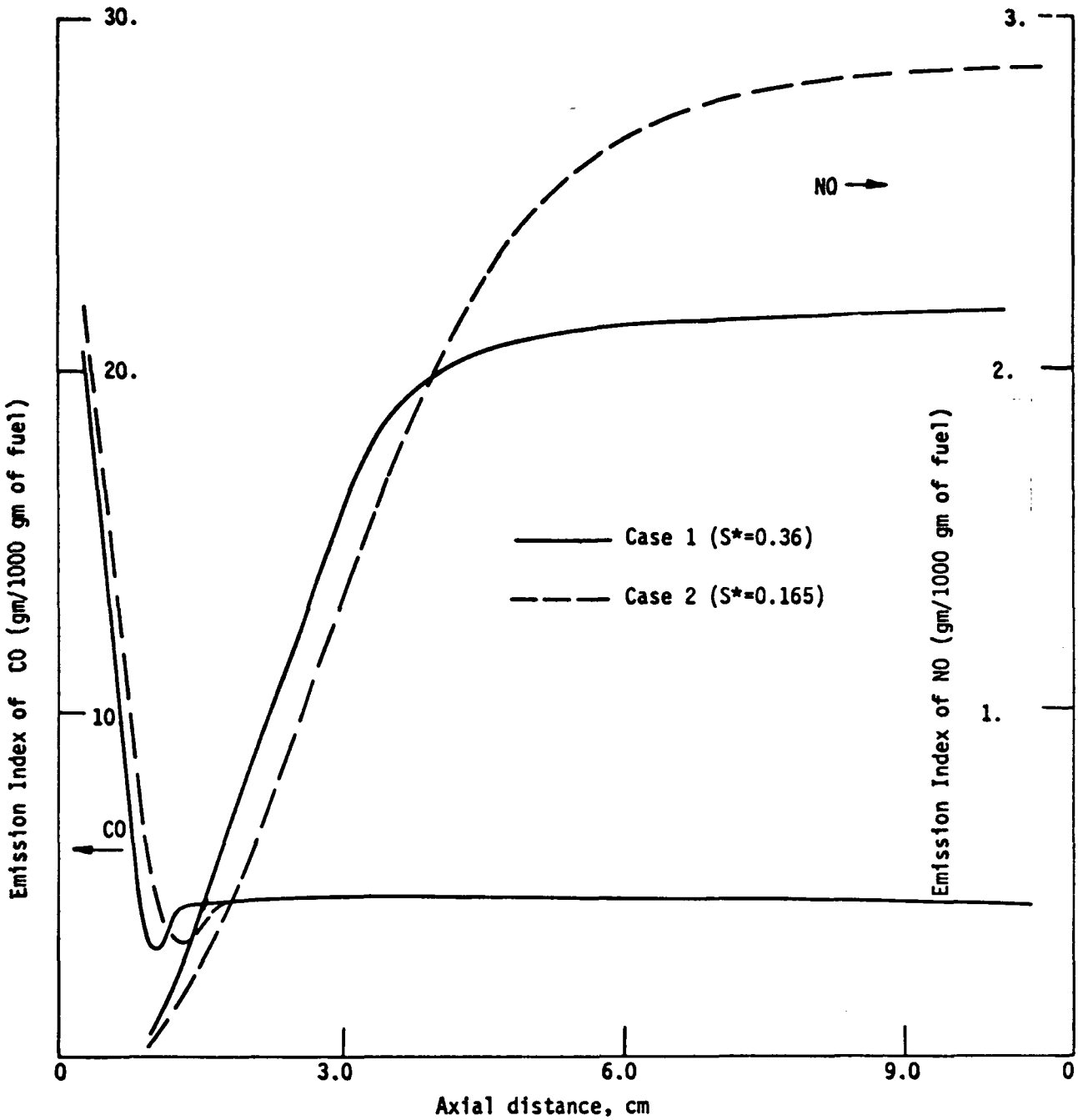

FIGURE 20. EFFECT OF SWIRL ON POLLUTANT PRODUCTION

CONCLUSIONS

Computations have been presented describing the mixing and combustion of swirling jets in a coaxial stream. It is demonstrated that the boundary layer equations represent the flow reasonably well until reversed flow is imminent.

For an isothermal jet with initial solid body rotation and uniform axial velocity the profiles of axial velocity exhibit a maximum that is shifted from the axis for swirl ratios $S^* > 0.43$. The onset of reversed flow is found at $S^* \approx 0.69$. For $0.25 < U_e/U_j < 1.5$ the edge velocity has little effect on the behavior of the flow. The calculations indicate that confining the flow with a constant pressure wall, or impressing a favorable pressure gradient on the coaxial flow, acts to reduce the severity of the centerline adverse pressure gradient created by the swirl decay.

The simple scalar eddy viscosity model of Rubel, including a potential core formulation, is shown to describe the behavior of weak swirling flow in the region $x/D > 15$ but is only in fair agreement with the data of Fejer et.al. in the near region. A slight modification of the model, employing radial uniformity of the eddy viscosity, is found to be sometimes advisable.

The effects of swirl on a burning hydrocarbon jet exhausting into a cold coaxial stream are shown to be intensified by the reduction of the jet density due to combustion. The enhanced mixing properties of high swirl flow produce rapid diffusion of the burning gases into the cold edge flow causing early cessation of the NO producing reactions. Computations show that doubling the initial jet swirl could reduce the NO production by 25%.

REFERENCES

1. Schwartz, I. R., "A Preliminary Investigation of Combustion with Rotating Flow in an Annular Combustion Chamber," NACA RM L51E25a.

2. Chervinsky, A., "Turbulent Swirling Jet Diffusion Flames," AIAA Journal, 7, 1877-1883, (October, 1969).

3. Fejer, A. A., Hermann, W. G. and Torda, T. P., "Factors That Enhance Jet Mixing," ARL 69-0175, (October 1969).

4. Syred, N., Chigier, N. A. and Beér, J. M., "Flame Stabilization in Recirculation Zones of Jets with Swirl," Thirteenth International Symposium on Comb., The Combustion Inst., Pittsburgh, pp. 617-624, (1971).

5. Beér, J. M., Chigier, N., Davies, T. W. and Bassindale, K., "Laminarization of Turbulent Flames in Rotating Environments," Combustion and Flame 1971, 16, pp. 39-45.

6. Lilley, D. G., "Prediction of Inert Turbulent Swirl Flows," AIAA Paper No. 72-699, (June 1972).

7. Rubel, A., "Some Effects of Swirl on Turbulent Mixing and Combustion," Advanced Technology Laboratories, Inc., NASA CR 1956, (1972).

8. Chigier, N. A. and Chervinsky, A., "Experimental Investigation of Swirling Vortex Motions in Jets," Trans. ASME, Ser. E, J. Appl. Mech. 34, pp. 443-451, (1967).

9. Niedzwiecki, R. W. and Jones, R. E., "Combustion Stability of Single Swirl-Can Combustor Modules Using ASTM-A1 Liquid Fuel," NASA TN D-5436, (October 1969).

10. Beér, J. M. and Chigier, N. A., "Combustion Aerodynamics," John Wiley and Sons, Inc., pp. 92-96, (1972).

11. Kleinstein, G., "On the Mixing of Laminar and Turbulent Axially Symmetric Compressible Flows," PIBAL Rep. No. 756, (February, 1963).

12. Zeiberg, S. and Bleich, G., "Finite Difference Calculation of Hypersonic Wakes," AIAA Journal, 2, 1396-1404, (1964).

13. Ferri, A., Moretti, G. and Slutsky, S., "Mixing Processes in Supersonic combustion," J. Soc. Ind. Appl. Math. 13, 229-258, (1965).

14. Newhall, H. K., "Kinetics of Engine-Generated Nitrogen Oxides and Carbon Monoxide," Twelfth International Symposium on Comb., The Combustion Inst., Pittsburgh, pp. 603-614, (1969).

REFERENCES (Continued)

15. Lavoie, G. A., Heywood, J. B. and Keck, J. C., "Experimental and Theoretical Study of Nitric Oxide Formation in Internal Combustion Engines," Combustion Science and Technology, 1, pp. 313-326, (1970).

16. Chinitz, W. and Baurer, T., "An Analysis of Non-Equilibrium Hydrocarbon Air Combustion," General Applied Science Laboratories, Inc., GASL TR 546, (1965).

NASA-Langley, 1973 —— 33 E-7332